

Existence of a Flat Phase in Red Cell Membrane Skeletons

Christoph F. Schmidt,* Karel Svoboda, Ning Lei,
Irena B. Petsche, Lonny E. Berman, Cyrus R. Safinya,†
Gary S. Grest

Biomolecular membranes display rich statistical mechanical behavior. They are classified as liquid in the absence of shear elasticity in the plane of the membrane and tethered (solid) when the neighboring molecules or subunits are connected and the membranes exhibit solid-like elastic behavior in the plane of the membrane. The spectrin skeleton of red blood cells was studied as a model tethered membrane. The static structure factor of the skeletons, measured by small-angle x-ray and light scattering, was fitted with a structure factor predicted with a model calculation. The model describes tethered membrane sheets with free edges in a flat phase, which is a locally rough but globally flat membrane configuration. The fit was good for large scattering vectors. The membrane roughness exponent, ζ , defined through $h \propto L^\zeta$, where h is the average amplitude of out-of-plane fluctuations and L is the linear membrane dimension, was determined to be 0.65 ± 0.10 . Computer simulations of model red blood cell skeletons also showed this flat phase. The value for the roughness exponent, which was determined from the scaling properties of membranes of different sizes, was consistent with that from the experiments.

Thermally fluctuating membranes assume curved and folded conformations, the properties of which are determined by competition between entropy and elastic energies (1, 2). Membranes, which are two-dimensional polymers, show properties remarkably different from those of linear polymers. One of these properties is an entropic long-range repulsion between membrane layers, which is a result of fluctuations in flexible liquid membranes caused by heat when their bending moduli are on the order of thermal energies. This interaction, predicted by theory (3) and demonstrated in recent synchrotron x-ray scattering experiments (4), can stabilize a multilayer phase with large interlayer distances (4–6). To date, tethered membranes have for the most part been treated theoretically. Examples of real systems are liquid crystalline gel phases of lipid bilayers (5), which are generally not flexible enough to allow large thermal fluctuations. Paradoxically, in tethered membranes that are more flexible, thermally induced local undulations have a stiffening effect on a large length scale, analogous to corrugations in a metal sheet.

More precisely, at low enough temperatures, the undulations of tethered membranes, coupled to in-plane phonon modes, give rise to anomalous effective large-scale elastic moduli. The bending elastic coefficient, κ , diverges, whereas the in-plane elastic shear and compressional moduli are predicted to soften to zero for membranes with progressively larger areas (7–9). This thermodynamic state has been termed the flat phase because, although the membrane exhibits roughness on small length scales, it appears increasingly flatter at larger length scales.

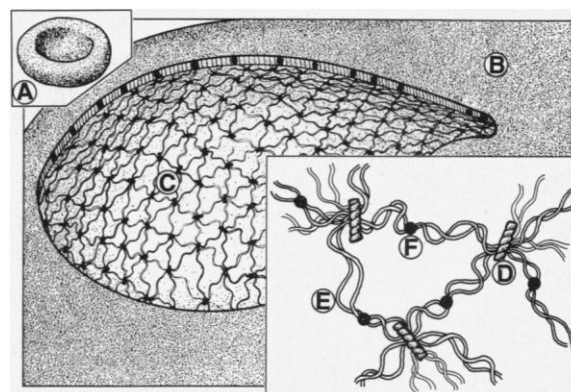
At a higher temperature, a phase transition to a crumpled phase has been predicted (1, 2, 10): this phase is an isotropic fractal, analogous to the random coils formed by linear polymers. Such a crumpled phase has not been found in computer simulations (11–13); this has led to the suspicion that excluded volume interactions, which are

not rigorously incorporated by theory, may prevent crumpling at all temperatures. On the other hand, graphite oxide membranes in good solvent are reported to assume crumpled conformations (14), although the data may not be sufficient to distinguish between crumpled and flat phases. Counterintuitively, crumpled and flat conformations in a membrane of a given size could appear to be very similar experimentally (15), if the fractal dimension of the crumpled phase is such that the local structure of both phases is similar.

We report light-scattering and synchrotron-based small-angle x-ray-scattering (SAXS) experiments with biological tethered membranes, namely, isolated red blood cell (RBC) membrane skeletons, together with extensive computer simulations of closed shell networks. Mammalian RBCs possess a multilayered membrane structure (Fig. 1), optimized to maintain the integrity of the cells while permitting large elastic deformations during blood circulation. The membrane skeleton, a shear elastic protein network, is attached to the cytoplasmic side of the (liquid) lipid cell membrane; the skeletons can be isolated from RBCs by detergent treatment (16). Screening of the electrostatic interaction of the charged skeleton shrinks the skeleton diameter by about a factor of 2 (17). Freshly isolated skeletons were observed under a light microscope as very flexible, roughly spherical shells (17).

Scattering experiments were performed on skeletons under two different buffer conditions (18) (Fig. 2, A and B). For the high salt sample, the plot of the static structure factor, $S(q)$ (Fig. 3, circles), obtained from the combined light-scattering and SAXS data (19), shows an oscillating scattering profile at small scattering vectors, q , typical of a solution of spherical shells, with the envelope of the oscillations falling off as approximately q^{-2} . The first minimum, at $q_m \approx 2.2 \times 10^{-4} \text{ \AA}^{-1}$, corresponds to a skeleton diameter of $2\pi/q_m \approx 2.9 \text{ \mu m}$. For

Fig. 1. Drawing of the red blood cell (RBC) membrane. Structure A is a whole red blood cell, diameter $\approx 8 \text{ \mu m}$. The outer lipid membrane (B), partially removed to expose the protein membrane skeleton (C), which consists of $\sim 70,000$ triangulated meshes (26). The membrane skeleton is a two-dimensional triangulated network, consisting mainly of actin oligomers (D), which form nodes, and spectrin tetramers (E), which form tethers. Ankyrin (F) makes a connection to the lipid membrane (27). Spectrin tetramers are flexible worm-like chains with a contour length of $\zeta \approx 2000 \text{ \AA}$ (21) and a persistence length of 100 to 200 \AA (17, 28). Both spectrin and actin have an excess of negative charge.



C. F. Schmidt and K. Svoboda, Departments of Cellular and Developmental Biology and Physics, Harvard University, Cambridge, MA 02138, and The Rowland Institute for Science, 100 Cambridge Parkway, Cambridge, MA 02142.

N. Lei, I. B. Petsche, C. R. Safinya, G. S. Grest, Exxon Research and Engineering Company, Annandale, NJ 08801.

L. E. Berman, National Synchrotron Light Source, Brookhaven National Laboratory, Upton, NY 11973.

*To whom correspondence should be addressed, at The Rowland Institute for Science.

†Permanent address: Materials and Physics Departments, University of California, Santa Barbara, CA 93106.

both salt concentrations, a crossover occurs at $q_c \approx 8 \times 10^{-4} \text{ \AA}^{-1}$ to a region of power law decay with an exponent of -2.4 ± 0.075 . The crossover occurs naturally in the description of the structure factor for the flat (but microscopically rough) membrane, as explained below. Although, in the two different salt concentrations, the overall skeleton diameters differ by about a factor of 2, the observed curve shape of $S(q)$ (for length scales between the diameter and the stretched-out mesh size of the skeleton) remains unchanged. This observation is consistent with the lack of a phase transition, which might have been expected to separate a flat phase for the low salt skeletons (with electrostatic repulsion between the spectrin subunits; Debye length, $\lambda_D \approx$

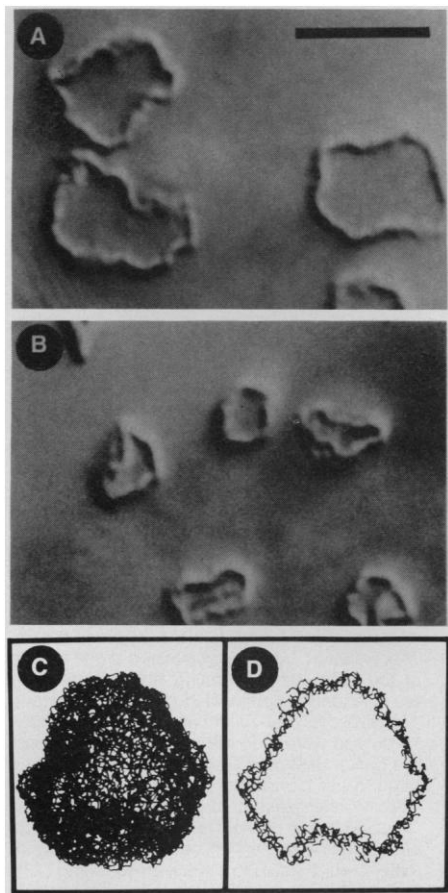


Fig. 2. Isolated RBC skeletons viewed under video-enhanced differential interference contrast (DIC) microscopy and simulated closed shell networks. The microscope and experimental procedures are described in more detail elsewhere (17, 18). **(A)** Skeletons in 50 mM monovalent cations. The mean diameter was $5.3 \pm 0.4 \text{ \mu m}$. **(B)** Skeletons in 1 M monovalent cations. The mean diameter was $2.6 \pm 0.3 \text{ \mu m}$. Scale bar = 5 \mu m for **(A)** and **(B)**. **(C)** Image of computer-simulated network with 16,002 monomers; average radius of gyration equals 28.8 monomer diameters. **(D)** Cross section through the center of the simulated network in **(C)**. Note similarity to shape of RBC skeletons.

15 \AA) from a crumpled phase for the high salt sample (in which the electrostatic interactions are screened; $\lambda_D \approx 3 \text{ \AA}$).

A marked difference between high and low salt samples was observed at scattering vectors that probed length scales smaller than the stretched network mesh size (which approximately equals the spectrin-tetramer contour length $\xi = 2000 \text{ \AA}$). Skeletons in low salt (50 mM Na^+) (Fig. 3, squares) show at $2 \times 10^{-3} \text{ \AA}^{-1} < q \approx 2\pi/\xi < 4 \times 10^{-3} \text{ \AA}^{-1}$ a crossover to a regime with a slope of $S(q)$ of about -1.3 on a log-log plot, characteristic of scattering from relatively rigid (due to the electrostatic interactions) single chains (20). This yields a value for ξ between 1500 and 3000 \AA , consistent with the spectrin-tetramer contour length of 2000 \AA (21). A further crossover at larger q to a Porod regime (22), where the protein-water interface determines the scattering, occurs at $q_P \approx 2.5 \times 10^{-2} \text{ \AA}^{-1}$. The length scale of $1/q_P \approx 50 \text{ \AA}$ gives a value for the membrane thickness T , which is consistent with the average thickness of an extended spectrin tetramer (30 to 60 \AA) (21). The pure Porod regime, characterized by $S(q) \propto q^{-4}$ in the case of a smooth interface for $q \gg 1/T$, was inaccessible because of solvent background scattering.

In contrast to the low salt data, which had clear crossovers, the plot of $S(q)$ for the high salt samples (Fig. 3, circles) displays power law decay over about two decades for $q > q_c \approx 8 \times 10^{-4} \text{ \AA}^{-1}$, up to $q \approx 1 \times 10^{-1} \text{ \AA}^{-1}$, beyond which the solvent background dominates. Because the spectrin-spectrin interactions in this case are

dominated by short-range excluded volume interactions, we believe that the membrane is closely packed laterally, so that the meshes become invisible. Consequently, the surface-like behavior extends to the length scales of the spectrin-tetramer thickness. Consistent with this, the skeleton surface area, the number of copies of spectrin and actin, and the molecular dimensions of these proteins suggest a closely packed membrane (17).

We compared our measured structure factor to model calculations. We used the static structure factor, $S_f(q_z, q_\perp, L)$, which describes an open-sided flat membrane of size L and roughness exponent ζ , with a height-height correlation function

$$\langle [h_z(\mathbf{x}_\perp) - h_z(\mathbf{x}'_\perp)]^2 \rangle = A |\mathbf{x}_\perp - \mathbf{x}'_\perp|^{2\zeta} \quad (1)$$

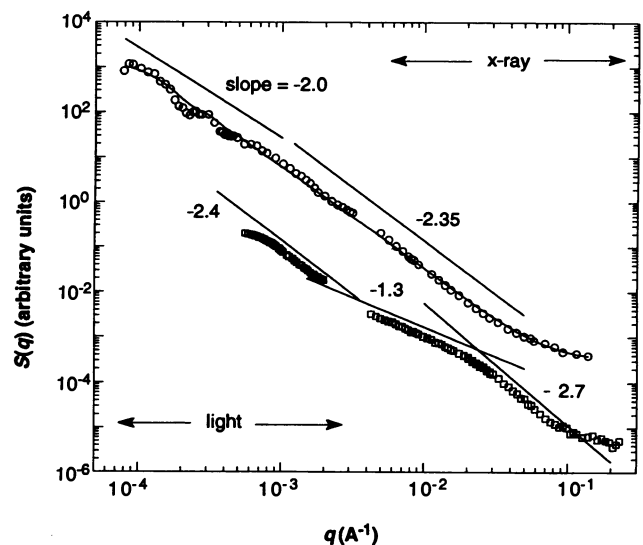
as calculated by Abraham and Nelson [equation 10 of (12), with the z -axis along the normal to the surface and \mathbf{x}_\perp in the membrane plane]. To fit the data, this structure factor is orientationally averaged:

$$S_f(q) \equiv \langle S_f(q_z, q_\perp, L) \rangle$$

$$= \int_{-1}^{+1} S_f(q_z = qx, q_\perp = q(1-x^2), L) dx \quad (2)$$

The value of $S_f(q)$ approaches a constant for $q \ll 1/L$. As pointed out by Sinha *et al.* (23), a section of lateral size r , cut out from a membrane described by $S_f(q)$, looks flat if $r > R_0 = A^{1/2(1-\zeta)}$ and rough (that is, amplitude of undulations greater than lateral size) if $r < R_0$. Accordingly, we expect $S_f(q) \sim q^{-2}$ for $1/L < q < 1/R_0$ (as we

Fig. 3. Static structure factor of detergent-extracted RBC skeletons (18) in high salt (1 M Na^+) buffer (circles) and low salt (50 mM Na^+) buffer (squares). Measured by light scattering ($-8 \times 10^{-5} \text{ \AA}^{-1} < q < -3 \times 10^{-3} \text{ \AA}^{-1}$ for high salt, $-5 \times 10^{-4} \text{ \AA}^{-1} < q < 2 \times 10^{-3} \text{ \AA}^{-1}$ for low salt) and small-angle x-ray scattering (SAXS) ($\sim 4 \times 10^{-3} \text{ \AA}^{-1} < q < 1.5 \times 10^{-1} \text{ \AA}^{-1}$) with synchrotron radiation. The curves have been vertically shifted for display. The solid line through the upper curve (high salt) is a fit of the orientationally averaged structure factor $S_f(q)$ of an anisotropic, flat tethered membrane plus a constant solvent background contribution to the data as described in the text. The averaged structure factor, $S_f(q)$, was convoluted with the experimental resolution function described previously (29). The convolution had a negligible effect because of the high resolution of the synchrotron. The goodness-of-fit parameter was $\chi^2 \approx 3$, and the fit resulted in a roughness exponent $\zeta = 0.65 \pm 0.10$, $L = 36,000 \pm 5,000 \text{ \AA}$, and $A = 106 \pm 10 \text{ \AA}^{2(1-\zeta)}$. This gives a crossover length $R_0 = A^{1/2(1-\zeta)} = 782 \text{ \AA}$. All other lines (numbers indicate slope) are guides to the eye as discussed in the text.



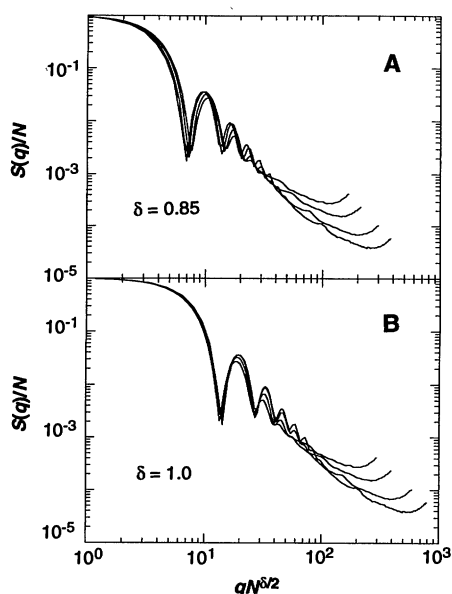


Fig. 4. Scaling plots for isotropically averaged $S(q)$ from computer simulations for closed shell tethered membranes as described in the text. The number of monomers in the network, N , ranged from 2,252 to 16,002. **(A)** Superposition of the high q parts of $S(q)$ (below the dispersion caused by finite monomer size) for different N for $\delta = 0.85$. **(B)** Superposition of the low q parts of $S(q)$ for $\delta = 1$.

observe in the envelope of the oscillations in Fig. 3), followed by a crossover into the rough regime with $S_f(q) \sim q^{-3+\zeta}$ for $q_c = 1/R_0 < q < 1/a$, where a is the molecular size cutoff. The $3 - \zeta$ power law behavior for $S_f(q)$ has been recently derived analytically by Goulian *et al.* (24). Our approximation for $S(q)$ will not reproduce the observed diffraction pattern of the relatively monodisperse spheres at large length scales (that is, small q 's) approaching the diameter D of the skeleton because the orientational averaging of the membrane sheet smooths out the oscillations. But, probing length scales smaller than D , we found that for larger q , $S_f(q)$ described the data well (Fig. 3, solid line through circles), with a roughness exponent $\zeta = 0.65 \pm 0.10$. Consistent with the data, the crossover from the smooth (q^{-2}) to the rough ($q^{-3+\zeta} = q^{-2.35}$) regime occurs at $q_c = 1/R_0 \approx 1.3 \times 10^{-3} \text{ \AA}^{-1}$.

Because simulations of a realistic model for the RBC skeleton are not feasible at this time, we studied instead a coarse-grained bead-spring model of flexible linear chains of eight monomers connected to form a geodesic. The overall size of the network varied between 2,252 and 16,002 monomers, the largest being about 50 times smaller than the experimental system (25). After equilibration, we measured the radii of gyration and height fluctuations of the membranes and found $\langle R_g^2 \rangle \propto N$ and $\langle h^2 \rangle \propto$

N^ζ , with $\zeta = 0.56 \pm 0.02$. The fluctuations and the structure of isolated RBC skeletons are qualitatively well captured by the computer simulation of a simple model of a closed shell network (Fig. 2, C and D). The results for $S(q)$ are shown in Fig. 4. The oscillations at low scattering vectors are more pronounced than in the experimental data as a result of the ideal monodispersity. The high q cutoff occurs relatively early, owing to the small system sizes. The power law behavior of $S(q)$ is shown by scaling plots (Fig. 4). The flat phase property of the networks is evident in the scaling of $S(q)$ at small q , where the curves and the first minima for different size networks scale as $qN^{1/2}$. The high q parts of the curves, on the other hand, up to the upper cutoff, scale as $qN^{\delta/2}$ with $\delta = 0.85$. This corresponds to a slope of $2/\delta = 2.35$ in the high q part of $S(q)$ and a roughness exponent $\zeta \approx 0.65$, which is consistent with the value determined from the experiments. Similar results were obtained for open membranes by Abraham and Goulian (15).

In conclusion, we find that the RBC skeleton provides an experimental realization of a tethered membrane and can be well described by a simple model network as being in an anisotropic structural phase, the flat phase. The local roughness of the membrane shows up in the orientationally averaged structure factor as a power law regime with an exponent of $-(3 - \zeta)$, with $\zeta = 0.65 \pm 0.10$. We take the fact that no crumpling transition was observed when the Debye screening length was changed in the solvent as evidence that such a transition is prevented by excluded volume interactions. Our data cannot rigorously exclude alternative models because the size and the size range of the studied membranes were relatively limited. No theoretical approach is available that takes into account all possible interactions between the protein strands in the network, but the large size and the shell-like conformation of the skeletons make it improbable that van der Waals and screened electrostatic interactions play more than a local role. Furthermore, the effect of the spherical topology of the skeletons has been neglected in our fitting of the structure factor. Building on the success of the simple model, more sophisticated theories and further experiments, especially those that address the dynamical properties of two-dimensional polymers, will lead to a deeper understanding of the exotic properties of tethered membranes.

REFERENCES AND NOTES

1. See *Statistical Mechanics of Membranes and Surfaces*, D. R. Nelson, T. Piran, S. Weinberg, Eds. (World Scientific, Singapore, 1989).
2. R. Lipowsky, *Nature* **349**, 475 (1991).

3. W. Helfrich, *Z. Naturforsch. Teil A* **33**, 305 (1978).
4. C. R. Safinya *et al.*, *Phys. Rev. Lett.* **57**, 2718 (1986); *ibid.* **62**, 1134 (1989).
5. See S. Leibler, in (1), pp. 45–103; *Nature* **348**, 586 (1990).
6. F. Larche *et al.*, *Phys. Rev. Lett.* **56**, 1700 (1986); R. Strey *et al.*, *J. Chem. Soc. Faraday Trans.* **86**, 2253 (1990); D. Roux, C. R. Safinya, F. Nallet, in *Modern Amphiphilic Physics*, A. Ben-Shaul, W. Gelbart, D. Roux, Eds. (Springer, New York, in press).
7. See D. R. Nelson, in (1), pp. 137–155.
8. ——— and L. Peliti, *J. Phys. (Paris)* **48**, 1085 (1987).
9. J. A. Aronovitz and T. C. Lubensky, *Phys. Rev. Lett.* **60**, 2634 (1988).
10. Y. Kantor and D. R. Nelson, *Phys. Rev. A* **36**, 4020 (1987).
11. F. F. Abraham, W. E. Rudge, M. Plischke, *Phys. Rev. Lett.* **62**, 1757 (1989); J. S. Ho and A. Baumgärtner, *ibid.* **63**, 1324 (1989); R. Lipowsky and M. Girardet, *ibid.* **65**, 2893 (1990).
12. F. F. Abraham and D. R. Nelson, *Science* **249**, 393 (1990).
13. G. S. Grest and M. Murat, *J. Phys. (Paris)* **51**, 1415 (1990).
14. X. Wen *et al.*, *Nature* **355**, 426 (1992).
15. F. F. Abraham and M. Goulian, *Europhys. Lett.* **19**, 293 (1992).
16. Y. Lange, R. A. Hadesman, T. L. Steck, *J. Cell Biol.* **92**, 714 (1982).
17. K. Svoboda, C. F. Schmidt, D. Branton, S. M. Block, *Biophys. J.* **63**, 784 (1992).
18. RBC skeletons were prepared by standard methods [M. P. Sheetz and D. Sawyer, *J. Supramol. Struct.* **8**, 399 (1978); B. W. Shen, R. Josephs, T. L. Steck, *J. Cell Biol.* **99**, 810 (1984)] with the following modifications. Ghosts [prepared according to J. T. Dodge, C. Mitchell, D. J. Hanahan, *Arch. Biochem. Biophys.* **100**, 119 (1963)] were mixed with one volume of 5 mM salt buffer, containing 20% Triton X-100, at 18°C. Skeletons were then prepared in two batches, one with a salt concentration of 50 mM monovalent cations (Na^+) and the other with 1 M Na^+ . Five minutes after the ghosts were mixed with detergent, a buffer containing 75 mM sodium phosphate (and 3 M NaCl for the high salt batch) was added to achieve a final concentration of 25 mM phosphate (and 1 mM NaCl, high salt batch). The samples were left at 18°C for 50 min and were then cooled to 4°C. Skeletons were separated from lipids and dissolved proteins by centrifugation (100,000g; 40 min; 10°C) through a 10 and 50% sucrose step gradient containing 0.5% (w/v) Triton X-100, 25 mM phosphate (and 1 M NaCl, high salt batch). The skeletons, which accumulated at the bottom of the tube without forming aggregates, were resuspended in a buffer of 25 mM phosphate (and 1 M NaCl, high salt batch) and 0.05% (w/v) Triton X-100 and were then dialyzed overnight against this buffer. Skeletons prepared this way lost their flexibility, in comparison to skeletons observed directly after detergent extraction (17). The "freezing" of the network is believed to be a result of the rearrangement of relatively few network tethers, which leads to a weak cross-linking (17).
19. The details of the sample holders and spectrometer configuration for the x-ray experiments have been described (29). The light-scattering experiments were repeatedly performed on two different instruments with consistent results: (i) At 488 nm and room temperature, scattering angles were between 2.5° and 20° on a custom-designed goniometer; (ii) at 632 nm and $T = 10^\circ\text{C}$, scattering angles were between 20° and 160° on a commercial goniometer. The plotted high salt light-scattering data were obtained with the first instrument, the low salt data with the second instrument.
20. P. G. De Gennes, *Scaling Concepts in Polymer Physics* (Cornell Univ. Press, Ithaca, NY, 1979).
21. D. M. Shotton, B. E. Burke, D. Branton, *J. Mol. Biol.* **131**, 303 (1979).
22. G. Porod, in *Small Angle X-Ray Scattering*, O. Glatter and H. C. Kratky, Eds. (Academic Press,

- New York, 1982), pp. 17–51.
23. S. K. Sinha, E. B. Sirota, S. Garoff, H. B. Stanley, *Phys. Rev. B* **38**, 2297 (1988).
 24. M. Goulian, N. Lei, J. Miller, S. K. Sinha, *Phys. Rev. A* **46**, R6170 (1992).
 25. The chains of the simulated tethered membrane were connected in a hexagonal array, except for 12 fivefold defects needed to close the sphere. The simulations were carried out using molecular dynamics with only excluded-volume interactions between the monomers. Details of the simulation can be found in (13) (also, I. B. Petsche and G. S. Grest, in preparation).
 26. C. W. M. Haest, *Biochim. Biophys. Acta* **694**, 331 (1982).
 27. S. C. Liu, L. H. Derick, J. Palek, *J. Cell Biol.* **104**, 527 (1987).
 28. B. T. Stokke, A. Mikkelsen, A. Elgsaeter, *Biochim. Biophys. Acta* **816**, 102 (1985).
 29. C. R. Safinya, in *Phase Transitions in Soft Condensed Matter*, T. Riste and D. Sherrington, Eds. (NATO ASI series B, Plenum, New York, 1989), vol. 211, pp. 249–270.
 30. We thank S. M. Block, D. Branton, P. A. Janmey, D. P. Kiehart, R. B. Meyer, M. Orkisz, and T. Tanaka for use of their equipment; T. C. Lubensky, D. R. Nelson, and S. K. Sinha for helpful discussions; H. C. Berg and S. M. Block for comments on the manuscript; C. Sun for the artwork in Fig. 1; J. Scarpetti for photographic work; and the Deutsche Forschungsgemeinschaft, the National Institutes of Health, the Department of Energy (DOE), and The Rowland Institute for Science for support. The SAXS experiments were carried out on the wiggler beam line X-25 at the National Synchrotron Light Source at the Brookhaven Laboratories, which is supported by DOE.

21 August 1992; accepted 25 November 1992

Photoinduced Polymerization of Solid C₆₀ Films

A. M. Rao, Ping Zhou, Kai-An Wang, G. T. Hager, J. M. Holden, Ying Wang, W.-T. Lee, Xiang-Xin Bi, P. C. Eklund,* D. S. Cornett, M. A. Duncan, I. J. Amster

The irradiation of oxygen-free, face-centered-cubic C₆₀ films with visible or ultraviolet light phototransformed C₆₀ into a different solid phase. Results from laser desorption mass spectroscopy, scanning electron microscopy, Raman and infrared spectroscopy, optical absorption, and luminescence indicate that a photopolymerization of the fullerene molecules within the film occurred.

The discovery of stable fullerenes, or carbon-cage molecules C_n ($n = 60, 70, \dots$), by Smalley, Kroto, and co-workers (1–3) has led to a new class of carbon-based solids with unusual properties (4, 5). At room temperature, the molecules in solid C₆₀ are centered on lattice positions of a face-centered-cubic (fcc) structure (6, 7) and are observed in nuclear magnetic resonance (NMR) experiments to be rapidly rotating about these lattice positions (8, 9). This unusual behavior is consistent with the weak intermolecular van der Waals bonding and the nearly spherical character of the C₆₀ molecule. In this report, we present results that indicate that the application of visible or ultraviolet (UV) light to solid C₆₀ polymerizes the structure, in that the molecules link together in a covalently bonded fcc structure. After phototransformation, the film

is no longer soluble in toluene but can be dissolved in boiling isodurene. Recently, Loy and Assink (10) reported a polymerized C₆₀ network. However, in their study, the C₆₀ molecules were linked by a hydrocarbon bridge formed during the reaction of C₆₀ in solution (toluene) with the diradical xyllylene. In photoconductivity studies of mixtures of C₆₀ and polystyrene, Wang (11) concluded that C₆₀ attaches to the polystyrene polymer.

On the basis of Raman scattering studies, we have reported (12) that Ar-ion laser radiation at 514.5 and 488.0 nm that exceeded ~ 50 mW/mm² appeared to initiate an irreversible transformation of fcc C₆₀ to a different solid phase with a richer Raman spectrum. In particular, the high-frequency A_g-symmetry “pentagonal-pinch” (PP) mode shifted at room temperature from 1469 to ~ 1460 cm⁻¹ (12), while the polarization ratio for this mode deteriorated from 100% in pristine C₆₀ to $\sim 80\%$ in the phototransformed phase (13). There has been some disagreement about the value of the PP-mode frequency (13). In our opinion, the value of 1469 cm⁻¹ has been incorrectly associated with only oxygen-contaminated C₆₀ (14, 15), and this view has recently been supported by others. Fourier transform Raman studies by Chase *et al.* (16) that used a yttrium-aluminum-garnet (YAG) laser with photon energy 1.06 eV, which is

less than the absorption threshold in C₆₀ (17, 18), confirm the 1469-cm⁻¹ PP-mode frequency for oxygen-free, pristine fcc C₆₀ obtained with a low-power Ar-ion laser beam (12, 13, 19).

The data presented here were taken on thin solid films of C₆₀ vacuum-deposited on either KBr, fused quartz, Si(100), or stainless steel substrates from 99% pure C₆₀ (Bluegrass Fullerenes, Inc., Lexington, Kentucky) first degassed in a vacuum of 10⁻⁵ torr for 3 to 6 hours at temperature (T) = 300°C. For the laser desorption mass spectroscopy (LDMS) studies, the C₆₀ film samples were deposited directly onto the end of stainless steel rods that could be transferred under a N₂ atmosphere into the mass spectrometer. The film-deposition apparatus resided in an He-atmosphere glove box (Vacuum Atmospheres, Inc., O₂ and H₂O < 1 ppm), and the exposure of the films to oxygen was therefore minimized. Inside the glove box, the film-substrate samples were transferred to a gas-tight cell with a quartz window that allowed the samples to be removed from the glove box and phototransformed by light from a 300-W Hg arc lamp or an Ar-ion laser. All of the phototransformed C₆₀ films studied received enough photon irradiation to shift the PP-mode frequency to 1460 cm⁻¹, and no trace of the initial 1469 cm⁻¹ peak remained. The film thickness (d) was typically in the range 1000 Å < d < 5000 Å.

A scanning electron microscope (SEM) image was taken of a phototransformed film that had been boiled in isodurene for several minutes (boiling point 198°C) (Fig. 1). The film had broken loose from the substrate, tearing along the line AB and folding over itself along line BC—that is, point A folded to point D. The area enclosed by ABC is associated with a residual film of phototransformed C₆₀ that was still attached to the substrate. Striations in the C₆₀ film that are evident in the image were not transferred from the glass substrate. The cracks in the film were also not transferred from the substrate and were not evident in the pristine film. They may be the result of heating during irradiation or a small contraction in the lattice parameter. Films such as the one shown in Fig. 1 survived boiling toluene (boiling point 111°C) for several hours but eventually dissolved in boiling isodurene.

We recorded LDMS spectra of phototransformed films (12-hour exposure to a 300-W Hg arc lamp) and pristine C₆₀ films (Fig. 2) that spanned the mass range of 720 atomic mass units (amu) (C₆₀) to 15,120 amu (21 × C₆₀). We took the spectra in Fig. 2, A and B, under similar desorption conditions: vacuum at $\sim 10^{-7}$ -torr, pulsed N₂ laser at wavelength of 337 nm focused to a spot 0.3 mm in diameter, pulse width of 5

A. M. Rao, P. Zhou, K.-A. Wang, Y. Wang, P. C. Eklund, Department of Physics and Astronomy, University of Kentucky, Lexington, KY 40506 and Center for Applied Energy Research, University of Kentucky, Lexington, KY 40511.

G. T. Hager, W.-T. Lee, X.-X. Bi, Center for Applied Energy Research, University of Kentucky, Lexington, KY 40511.

J. M. Holden, Department of Physics and Astronomy, University of Kentucky, Lexington, KY 40506.

D. S. Cornett, M. A. Duncan, I. J. Amster, Department of Chemistry, University of Georgia, Athens, GA 30602.

*To whom correspondence should be addressed.